World Journal of Advanced Engineering Technology and Sciences
eISSN: 2582-8266
Cross Ref DOI: 10.30574/wjaets
Journal homepage: https://wjaets.com/

(RESEARCH ARTICLE)

Check for updates

# Modeling of 3D inhomogeneous human body from medical images

Ihab ELAFF *

*Computer Science and Engineering Department, College of Engineering, Qatar University, Qatar.*

World Journal of Advanced Engineering Technology and Sciences, 2025, 15(02), 2010-2017

Publication history: Received on 05 April 2025; revised on 14 May 2025; accepted on 17 May 2025

Article DOI: https://doi.org/10.30574/wjaets.2025.15.2.0772

## Abstract

This study presents a comprehensive approach for modeling the human torso as an inhomogeneous volume conductor using medical imaging data. CT scans of a male human subject were processed through a sequence of image segmentation and boundary extraction techniques to construct both surface and volume models of major organs, including the lungs, liver, and bones. The surface model relies on isotropic assumptions for each organ, while the volume model enables future incorporation of tissue anisotropy. Manual and automatic techniques were combined to extract organ contours, smooth boundaries, and construct three-dimensional representations. The resulting model provides a realistic anatomical structure suitable for advanced biomedical simulations and electrical activity mapping.

**Keywords:** Inhomogeneous volume conductor; Human torso modeling; 3D organ reconstruction; Anatomical modeling; Tissue conductivity

## 1. Introduction

The body can be modeled either as a homogenous or as an inhomogeneous volume conductor. For a homogenous volume conductor, it is assumed that all organs including the blood volume inside ventricles have the same physical parameters (conductivity, permeability). In contrast, for an inhomogeneous volume-conductor, each organ has its own parameters. Inhomogeneity of the body affects the produced surface potential as introduced by Gulrajani and Mailloux [1], where it was shown that the blood mass has the largest effect on the body surface potential. These studies describe the detailed development of the human torso that is used in modeling human heart activation [2].

All of the organs in reality are anisotropic materials. Some tissues such as the skeletal muscles have strong anisotropic properties while others like liver and lungs have almost isotropic properties [3]. Including organ anisotropy requires a huge amount of data that describes the composition of each organ. However, considering the organs to be an isotropic material is acceptable and this will simplify the modeling [3].

Some models describe the volume conductor (the body) in terms of an approximate shape [4], but the most widely used is the realistic torso shape. The realistic torso shape models are either a homogenous volume conductor as described in the literature [5 – 10] or the widely used inhomogeneous volume conductor as described in [11 – 21].

With the rapid development of medical imaging, it is now possible to obtain a massive amount of image data for human anatomy. These images come from a variety of medical imaging modalities, including X-ray, Computed Tomography (CT), Magnetic Resonance Imaging (MRI), and Ultrasound. These techniques provide the ability to look inside the body in a non-invasive manner. Modeling of the body as an isotropic-inhomogeneous volume conductor is usually done by either CT-scan data or MRI data because they are able to provide high-resolution 2D grey-level slices, which help to distinguish between different organs inside the body.

* Corresponding author: Ihab ELAFF

## 2. Methods

### 2.1. Modeling Block Diagram

Modeling of the body and the heart of a human can be summarized as shown in the block diagram (Figure 1) on the following page. There are two input datasets, the CT-scan of a human thorax, and the DT-MRI dataset of a human heart. These datasets pass through several processing stages to get finally a model for inhomogeneous human body including the torso, the lungs, the liver, some bones, and other organs, as well as the heart's ventricles which are modeled as anisotropic material that containing the conduction system.

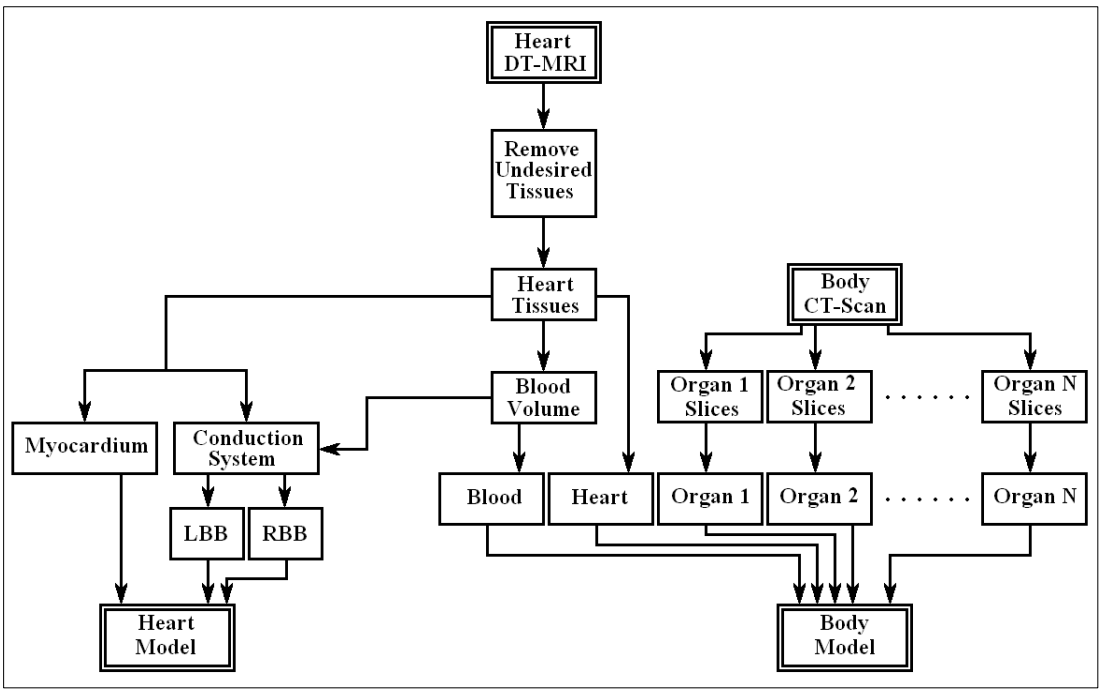


**Figure 1** Block diagram of modeling the body and the heart

In modeling the human body, it is considered to be an inhomogeneous volume conductor, so it is necessary that the different organs has its own parameters (conductivity, permeability, … etc). The approach taken has been to use CT scans for a male human of average size [22]. By using image processing techniques (thresholding, manual segmentation, boundary thinning, boundary smoothing, edge tracing), it was feasible to split and fine tune different organs in each image and finally reconstruct the body as a 3D mesh. The heart is removed from the body model because it is necessary to be modeled in more detail and the CT scans are not being capable of providing this level of detail.

The body has been represented in two different models, a volume model and a surface model. The surface model is used when each organ inside the body is considered to have isotropic tissues properties, while the volume model can be used for any type of tissues and it is implemented for further upgrades when the anisotropy data of organs are available.

### 2.2. Image Sensation

The surface model of the human body was reconstructed by splitting CT scan images into groups of images (Figure 2), where each group represents slices of a particular organ.

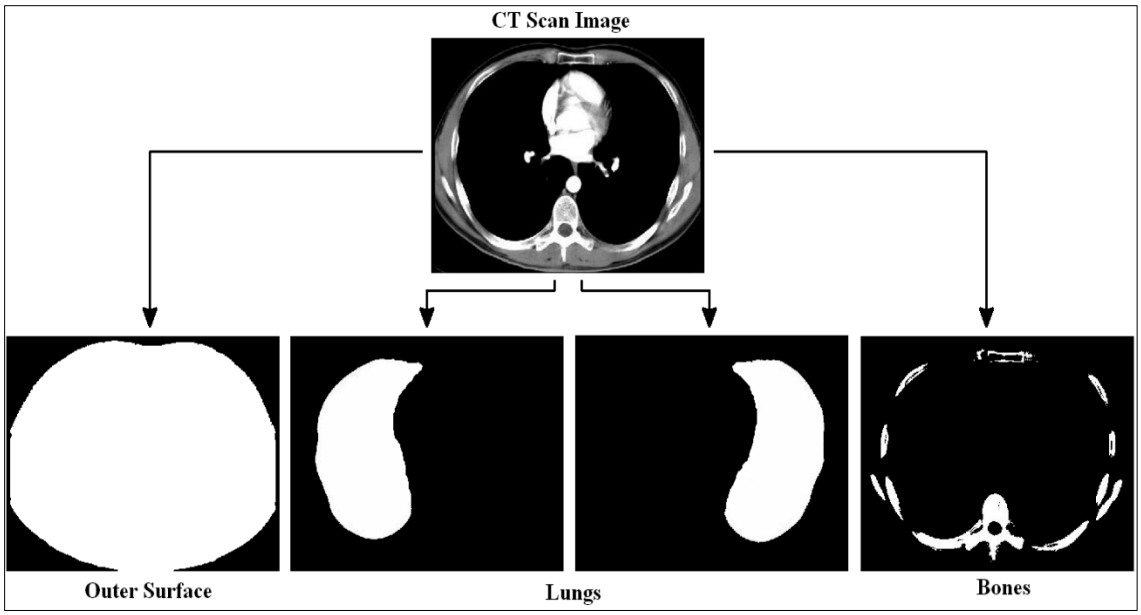


**Figure 2** Splitting of CT scan into different images groups

Different thresholds have been taken according to Table 1 to separate organs so that binary image slices are produced as the following steps:

All images are converted to grayscale images of 256 color palettes by assigning the pixel to the average value of its Red, Green and Blue components.

A threshold is taken at the level 10 of the grayscale levels to separate the background from the body area in each slice.

Some areas, such as Lungs area, are filled with white color manually to produce finally a mask (outer surface) that includes the area of interest for the next stages of processing. This is also used for defining body torso contours.

A slice of an organ is extracted from the grayscale images by assigning all mask points that are included in the organ range with the white color and other points to background color (black).

The additional noise and undesired detail in each slice are removed manually.

The area of the organ in each slice is then removed from the mask for next organs processing (the order that was taken is: bones, then lungs, the liver and then other organs)

The boundary of object in each image is smoothed automatically (keeping pixel that has more than 4 neighbors).

The boundary of the organ slice is then deleted twice to reduce the size of the organ to not to overlap the boundary of the neighbor organs (to be sure about full separation of organs in the reconstructed model).

The model that has been developed includes the lungs, the liver, some bones, other organs, as well as the body torso.

**Table 1** Different threshold values to separate organs

| Organ | Threshold Range |
|---|---|
| Bones | 195 – 255 |
| Liver | 130 – 170 |
| Others | 100 – 240 |
| Lungs | 0 – 50 |

Segmentation also can be done using some algorithms such as Otsu [23], K-Means [24] and Fuzzy C-Means [25] for automated process where number of clusters is set to 5 clusters. Much enhanced segmentation model can be obtained based on DTI images and the non-unique solution of segmentation problem can be reduced by applying uni-stable methods [26, 27] for more accurate and precise boundaries where Medical Image Segmentation Utility (MISU) [28] can be used for that task.

### 2.3. Reconstruct Organs

For each image (of every object in the dataset) (Figure 3-a), the boundary of the slice is traced automatically as an 8 connected edge that surround the object (Figure 3-b) and divided automatically into equal segments (Figure 3-c).

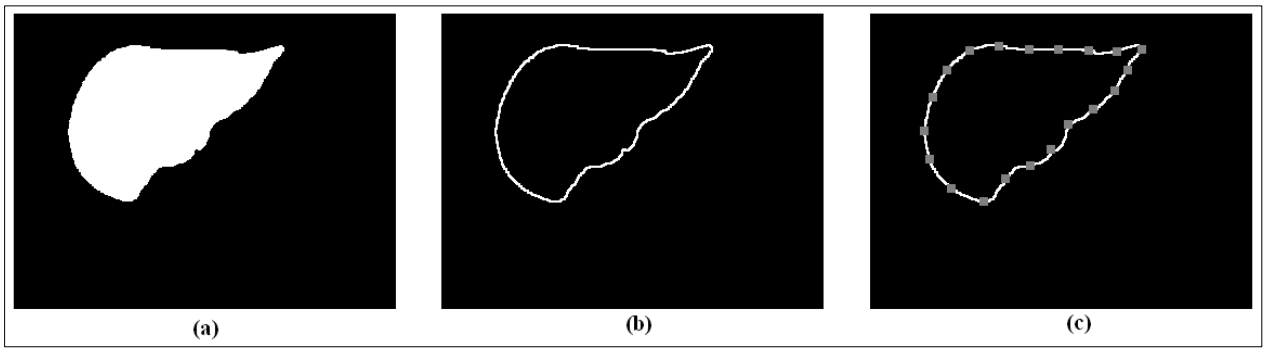


**Figure 3** Boundary tracing and splitting of an object. (a) the original image. (b) detecting the boundary of object inside the image. (c) splitting the boundary into equal segments

The boundary of the slice is determined as follows

- The image is scanned until a non-background pixel is found. This is set to Current Pixel and marked as an edge point and also as a start point.
- The previous scanning point (which is a background point) is set to be the Scanning Pixel.
- Starting from the Scanning Pixel, the eight neighbors of the Current Pixel are checked in order either clockwise or counter clockwise until a non-back ground pixel is found and set as Found Pixel.
- The Scanning Pixel is set to the Current Pixel and the Current Pixel is set to Found Pixel.
- If the Current Pixel is unmarked, then it is marked as an edge pixel and the procedure is repeated from step 3, else terminate the loop.

The number of segments varies according to the required modeling resolution and the number of segments selected for this study was 50 segments per contour. Increasing the resolution produces a smoother surface, but also requires longer times for processing. Locations that link these segments are considered to be the X and Y components of a vertex of an object in that slice. The slice number is scaled to be the Z component of that vertex (where X, Y and Z define the location of a vertex in 3D space).

## 3. Results

Finally, vertices which are collected from each group of images are linked together in an appropriate manner to reconstruct an organ (Figure 4).

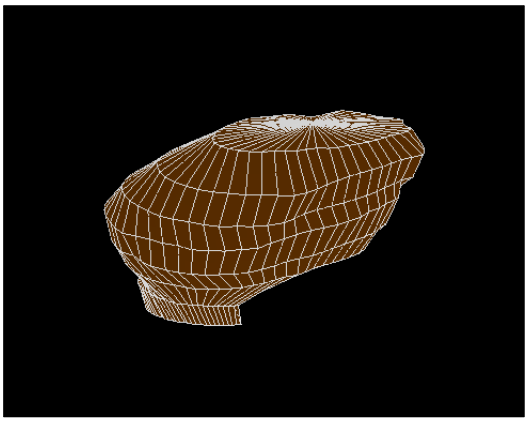

**Figure 4** Reconstructing of organ (e.g. liver)

All organs inside the torso are considered closed surface objects. There were difficulties in modeling chest ribs so they were neglected. Finally, the full model of the body that was generated is as shown in Figure 5.

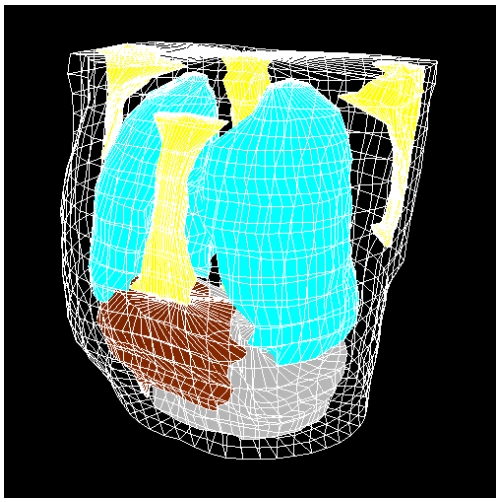

**Figure 5** Reconstructing Human Torso as surfaces model from CT scans

The volume model of the body (Figure 6) is reconstructed by considering the whole area of each object in the image where a volumetric element (e.g. cube) is inserted in the location of each pixel. Conductivity of each organ is taken according to values presented in the literature [29] (Table 2).

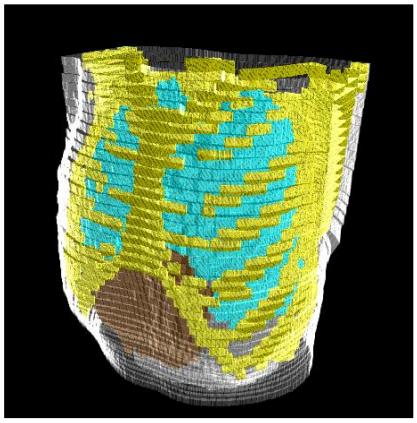

**Figure 6** Reconstructing Human Torso as volumes model from CT scans

**Table 2** Different values of tissues and organs resistivity and conductivities [29]

| Organ/Tissue | Resistivity (Ωcm) | Conductivity (mS/mm) |
|---|---|---|
| Skeletal muscle | 400 | 25 |
| Fats | 2000 | 5 |
| Bone | 2000 | 5 |
| Liver | 600 | 16.7 |
| Left lung, right lung | 1325 | 7.5 |
| Blood masses | 150 | 66.7 |
| Other tissues and organs | 460 | 21.7 |
| Heart muscle | 450 | 22.2 |

A revised version of Figure 1, which shows the modeling of the body torso and some organs inside the human body using CT images is shown below (Figure 7).

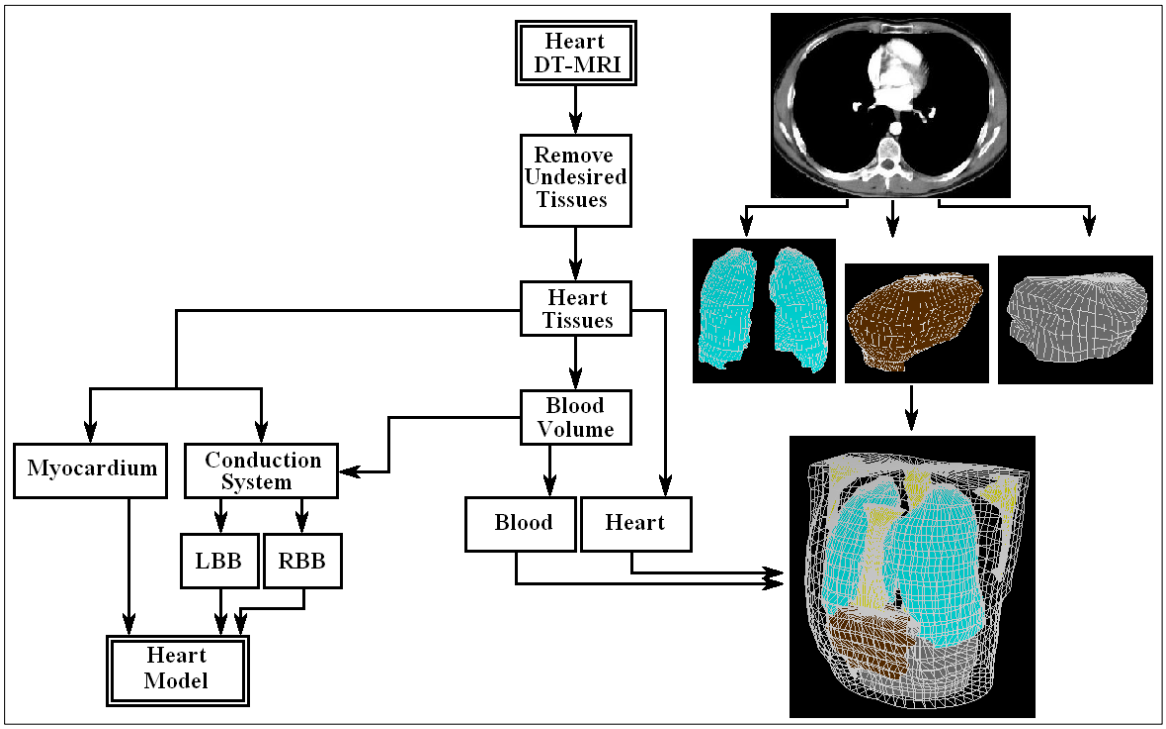


**Figure 7** Block diagram of modeling the body and the heart after finishing the body model

## 4. Conclusion

The developed anatomical model successfully represents the human torso as an inhomogeneous volume conductor using CT imaging data. By applying detailed segmentation and reconstruction methods, individual organs were modeled with precision and fully separated within the 3D structure. The resulting surface and volume models offer flexibility for future expansion, including anisotropic characterization and integration with heart modeling. This framework lays a foundation for improved physiological simulations, particularly in understanding body surface potentials and supporting biomedical research in electrophysiology and imaging-guided diagnostics.

## References


[1] R.M. Gulrajani and G.E. Mailloux "A simulation study of the effects of torso inhomogeneities on electrocardiographic potentials, using realistic heart and torso models" Circ. Res., (1983); 52:45-56.

[2] I. ELAFF (2018) "Modeling of realistic heart electrical excitation based on DTI scans and modified reaction diffusion equation," Turkish Journal of Electrical Engineering and Computer Sciences: Vol. 26: No. 3, Article 2. https://doi.org/10.3906/elk-1710-118J.

[3] Malmivuo and R. Plonsey "Bioelectromagnetism: Principles and Applications..." Oxford Univ. Press, (1995); ISBN: 0195058232.

[4] V. Soundararajan and W.G. Besio "Simulated Comparison of Disc and Concentric Electrode Maps..." IJBEM, (2005); 7(1):217-220.

[5] K. Simeliusa, J. Nenonena, M. Horácekb "Modeling Cardiac Ventricular Activation" Inter. J. of Bioelectromagnetism, (2001); 3(2):51 - 58.

[6] V. Jazbinsek, R. Hren, and Z. Trontelj "High resolution ECG and MCG mapping: simulation study..." Bulletin of the Polish Academy of Sciences, (2005); 53(3): 195-205.

[7] L.W. Wang, H.Y. Zhang, P.C. Shi "Simultaneous Recovery..." Computers in Cardiology, (2006);33:45-48.

[8] X. Zhang, et al. "Noninvasive 3D electrocardiographic imaging..." Am J Physiol Heart Circ Physiol (2005); 289: H2724–H2732.

[9] G. Li, X. Zhang, J. Lian, and B. He "Noninvasive Localization of the Site of Origin of Paced Cardiac Activation in Human by Means of a 3-D Heart Model" IEEE Trans. Biomed. Eng. (2003); 50(9): 1117-1120.

[10] Z. Liu, C. Liu, and B. He "Noninvasive Reconstruction..." IEEE Trans. Med. Imag. (2006); 25(10): 1307-1318.

[11] D.S. Farina, et al. "Personalized Model of Cardiac Electrophysiology..." IJBEM (2005);7(1): 303-306.

[12] M. Seger "Modeling the Electrical Function of the Human Heart", Ph.D. Thesis, University for Health Sciences, Austria (2006).

[13] M. Lorange, and R. M. Gulrajani "A computer Heart Model Incorporating Anisotropic Propagation" Journal of Electrocardiology, (1993);26(4):245-261.

[14] C. Hintermuller "Development of a Multi-Lead ECG Array..." Ph.D. Thesis, Austria (2006).

[15] M. Seger, et al. "Non-invasive Imaging of Atrial Flutter" Computers in Cardiology (2006);33:601-604.

[16] T. Berger, et al. "Single-Beat Noninvasive Imaging of Cardiac Electrophysiology..." JACC (2006);48:2045-2052.

[17] L. Cheng "Non-Invasive Electrical Imaging of the Heart", Ph.D. Thesis, The University of Auckland, NZ (2001).

[18] C.G. Xanthis, et al. "Inverse Problem of ECG for Different Equivalent Cardiac Sources" PIERS Online, 2007; 3(8): 1222-1227.

[19] B.E. Pfeifer "Model-based segmentation techniques..." Ph.D. Thesis, Austria (2005).

[20] B. He, and D. Wu "Imaging and Visualization of 3-D Cardiac Electric Activity" IEEE Tran. Inf Tech. Biomed. 2001; 5(3): 181-186.

[21] B. He, C. Liu ,and Y. Zhang "Three-Dimensional Cardiac Electrical Imaging..." IEEE Trans. Biomed. Eng. (2007); 54(8): 1454-1460.

[22] The Radiological Institute at the University Hospital of Erlangen Site "http://www.idr.med.uni-erlangen.de/COMPARE/CTThorax.htm", May 2025.

[23] Otsu N. A threshold selection method from gray-level histograms. IEEE T Syst Man Cyb 1979; 9: 62–66.

[24] Wagsta K, Cardie C, Rogers S, Schroedl S. .Constrained K-means Clustering with Background Knowledge. In: Proceedings of the Eighteenth International Conference on Machine Learning (ICML 2001), Williams College, Williamstown, MA, USA, June 28 - July 1, 2001. Morgan Kaufmann 2001 pp. 577-584.

[25] Wen Y, He L, Von Deneen KM, Lu Y. Brain tissue classification based on DTI using an improved Fuzzy C-means algorithm with spatial constraints. Magn Reson Imaging 2013; 31: 1623-1630.

[26] I. ELAFF, I. A. EL-KEMANY, and M. KHOLIF "Universal and stable medical image generation for tissue segmentation (The unistable method)," Turkish Journal of Electrical Engineering and Computer Sciences: Vol. 25: No. 2, Article 32, 2017. https://doi.org/10.3906/elk-1509-100.

[27] I. Elaff, "Medical Image Enhancement Based on Volumetric Tissue Segmentation Fusion (Uni-Stable 3D Method)", Journal of Science, Technology and Engineering Research, vol. 4, no. 2, pp. 78–89, 2023. https://doi.org/10.53525/jster.1250050.

[28] I. ELAFF, "Medical Image Segmentation Utility (MISU)" https://github.com/Ihab-ELAFF/Medical-Image-Segmentation-Utility-MISU. May 2025

[29] P. Kauppinen, et al. "A software implementation for detailed volume conductor modelling..." Computer Methods and Programs in Biomedicine (1999); 58: 191–203.